Energy Minimization of Mixed Argon–Xenon Microclusters Using a Genetic Algorithm

W. J. PULLAN*

Department of Mathematics and Computing, Central Queensland University, Rockhampton, Queensland, 4702, Australia

Received 10 July 1996; accepted 25 September 1996

ABSTRACT: This article describes a parallel real-coded genetic algorithm implemented to find global minimum energy structures of microclusters of non-bonded argon and xenon atoms. Using appropriate genetic operators, the genetic algorithm was able to find minimum energy structures for microclusters of two to twenty atoms, in all possible combinations of argon and xenon.
 J Comput Chem **18:** 1096–1111, 1997

Keywords: global optimization; genetic algorithm; molecular conformation

Introduction

Atomic microclusters are currently an active field of theoretical and experimental research. Microclusters are aggregates of atoms or molecules, sufficiently small so that a significant proportion of these units are present on the surface of the microcluster. Theoretical investigations of microclusters address the following optimization problem:

> *Given N particles, interacting with two-body central forces, find the configuration in three-dimensional Euclidean space for which the total potential energy attains its global minimum.*

*Present address: University of Colorado at Boulder, Department of Computer Science, Campus Box 430, Boulder, CO 80309-0430.

Correspondence to: W. J. Pullan

Simplifications normally used are that many-body and angle dependent interactions are ignored, quantum effects are not taken into account and all particles are assumed to be spherical and the same size. Using these simplifications, the potential energy of an N atom microcluster can be written as:

$$V = \sum_{i=1}^{N-1} \sum_{j=i+1}^{N} v(r_{ij})$$

where r_{ij} is the Euclidean distance between atoms i and j, and $v(r_{ij})$ is the pair potential between atoms i and j. From a molecular point of view, the potential energy of a microcluster can be described by a hypersurface, normally referred to as a potential energy surface, of high dimensionality ($3N - 6$, where N is the number of atoms in the microcluster). The geometry of the microcluster's most stable conformation is the geometry corresponding to

 CCC 0192-8651 / 97 / 081096-16

the global minimum of the potential energy surface. Even with the simplifying assumptions, the minimization of the potential energy of a microcluster is very difficult to achieve as it is a nonconvex optimization problem involving numerous local minima. In fact, Hendrickson[1] has shown that even simple versions of the problem are *NP*-complete; that is, the expected time to find the global minimum increases exponentially with the dimension of the problem.

This article describes a parallel real-coded genetic algorithm (GA) which has been applied to the problem of finding minimum energy configurations of microclusters containing a mixture of argon and xenon atoms. The remainder of this section describes pure and mixed microclusters and presents a review of optimization methods that have been used to find their minimum energy configurations. A later section describes the implementation of the computational method used in this study. The results are then presented and discussed. Finally, the conclusions are presented in the final section.

PURE MICROCLUSTERS

As pure microclusters are composed of a single type of atom, the scaled Lennard–Jones pair potential is normally used to investigate their properties. This pair potential is shown in Figure 1 and defined by

$$v(r) = (1/r)^{12} - 2(1/r)^{6}$$

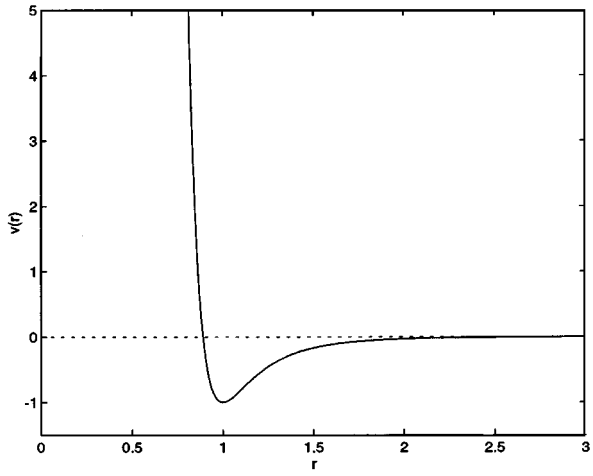

FIGURE 1. Scaled Lennard–Jones pair potential, $v(r) = (1/r)^{12} - 2(1/r)^{6}$.

where r is the distance between the atoms. The first term is an approximation for the repulsive component (for which no rigorously derived expression exists), whereas the second attraction term can be rigorously derived for spherical, chemically saturated atoms.

An extensive review of the theory and structure of microclusters is presented in Hoare[2] where the question of the number, and types, of local minima possible on the potential energy surface for a microcluster is addressed. In terms of the energy function, the only quantitative statement that can be made is that, for a pure N atom microcluster with $v(r)$ as the pair potential, there exists a weak lower bound given by:

$$-N(N-1)/2$$

That is, a simplex in $N-1$ dimensions in which all atoms are nearest neighbors (distance 1 apart), gives the lowest energy possible. Liao[3] has shown that, for an N atom microcluster with $v(r)$ as the pair potential, a global minimum exists and the corresponding configuration is contained within a sphere, centered at the origin, and of radius:

$$(N-1)\sqrt{N-1}$$

For smaller microclusters, with $v(r)$ as the pair potential, globally minimum configurations are:

- Two atoms—separated by 1 unit.
- Three atoms—an equilateral triangle, each side 1 unit.
- Four atoms—a tetrahedron, each side 1 unit.
- Five atoms—a triangular bipyramid, slightly contracted along the symmetry and distended in the symmetry plane.
- Six atoms—the regular octahedron with slightly contracted sides.
- Seven atoms—part of a regular icosahedron with slightly distended edges and contracted axial distances.

For more than seven atoms, minimum energy configurations are based on icosahedral lattice structures.[4]

Determining the number of distinct local minima (which includes the global minimum) is not straightforward for microclusters due to the symmetries involved. Minima associated with structures which differ only in labeling of atoms must first be eliminated. In addition, minima that are associated with structures which are equivalent

under proper symmetry operations in three dimensions must also be eliminated. Finally, there are some pairs of structures which must be eliminated as they share the same potential energy and the same distances between atoms (to within atom numbering) but are not superimposable under normal symmetry operations. The total number of distinct local minima, $m(N)$, for microclusters consisting of 2 to 13 atoms is 1, 1, 1, 1, 2, 4, 8, 18, 57, 145, 366, and 988, respectively, and is approximated by[2]:

$$m(N) = \exp(-2.5176 + 0.3572N + 0.0286N^2)$$

OPTIMIZATION OF PURE MICROCLUSTERS

Lattice-Based Methods

Hoare et al.[2,5–7] developed a general growth algorithm and used it to generate large numbers of stable structures, mainly in the range $N \leq 55$. These were compared to find the lowest energy structures, which in turn became candidates for the globally minimum structures. Hoare and Pal[5] observed that, while what they termed as the ''icosahedral growth sequence'' did not, in general, produce minimal structures, icosahedral subunits did appear regularly in relaxed configurations generated by other sequences.

Using results from the Hoare and Pal study, Northby[4] produced what is currently the most successful algorithm for minimizing Lennard–Jones microclusters. At a high level of abstraction, Northby's algorithm proceeds as follows:

- For N atoms, define the set S of all possible icosahedral shell lattices (with inner shells densely packed).
- Define a potential function for optimizing this discrete problem (i.e., optimizing where each atom must remain on a lattice vertex). Northby used a ''square well'' potential of the form:

$$v(r) = \begin{cases} 0 & 0 \leq r \leq 0.8 \\ -1 & 0.8 < r < 1.2 \\ 0 & 1.2 \leq r \leq \infty \end{cases}$$

- For each lattice in the set S, perform a lattice-based search optimization to identify minimum energy lattice-based configurations.
- Using the Lennard–Jones potential function, optimize all geometrically distinct structures using a gradient search method.

Clearly, the critical assumption in Northby's algorithm is that a well-defined set of lattice structures contains at least one initial cluster configuration which relaxes to the cluster configuration corresponding to the global minimum of the potential energy.

Simulated Annealing

Wille[8] applied simulated annealing (SA) to Lennard–Jones microclusters for $4 \leq N \leq 25$. For small microcluster sizes ($4 \leq N \leq 13$), one atom was kept in a fixed central position, to eliminate translational degrees of freedom, and for the larger ones ($14 \leq N \leq 25$) 13 atoms were kept in a central icosahedral environment during annealing. As is common with the use of SA, the difficult part is the determination of the cooling schedule. A cooling rate that is too slow is time consuming, while a fast cooling rate will lead to minima other than the global minima. To analyze the influence of the cooling schedule on the final state, Wille performed a number of simulations on 13-atom microclusters making the number of possible steps per atom at each temperature equal to $K(1 - \log T)$, where $K = 200$ and 2500 with the temperature reduction factor being 0.9. In the first case, 3 of 30 runs produced the isosahedral structure, whereas in the second case 4 of 5 runs gave this result. This indicates how the likelihood of detecting the global minimum increases with decreasing cooling rate.

Xue[9] implemented a two-level parallel version of simulated annealing for use with an icosahedral lattice-based search technique which had increased computational efficiency over that used by Northby. Xue's basic (nonparallel) two-level simulated annealing algorithm uses a local optimizer to determine the local minimum for the catchment basin within which each generated point lies. New points are moved to by comparing the local minima of the associated catchment basins rather than the values associated with the actual points. When the temperature gets low, two-level simulated annealing still accepts moves that lead to worse function values, but these moves all lead to better (or the current) local minima. That is, the two-level simulated annealing algorithm can easily climb up a hill at any temperature, but is very unlikely to

move into the catchment basin of a worse local minima when the temperature is low.

Genetic Algorithms

Hartke[10] used a genetic algorithm (GA) to find global minimum energy structures for four atoms. An encoding method, using just four parameters to specify the four-atom configuration, allowed a standard GA to find the global minimum energy. Mestres and Scuseria[11] were able to find global minimum energy configurations for Lennard–Jones microclusters of up to 13 atoms. More recently, Deaven and Ho[13] used a real-coded GA with tailored genetic operators to find the global minimum energy for fullerene structures up to C_{60} and Gregurick et al.[12] used a modified deterministic/stochastic genetic algorithm to find all currently accepted global minima for Lennard–Jones atomic clusters in the range $2,\ldots,29$. However, this method required a seed growth method for generating initial structures for all clusters containing more than 20 atoms. More recently, Deaven et al.,[19] using a real-coded GA with innovative phenotype genetic crossover operators, were able to find all global minimum energies for Lennard–Jones pure atomic clusters in the range \$2, . . . , 100\$ including new minima for 38, 65, 69, 76, 88 and 98 atomic clusters.

MIXED MICROCLUSTERS

While all the studies mentioned above have focused on pure microclusters, investigations have also been performed on microclusters containing a mixture of argon and xenon atoms. For these microclusters, the scaled Lennard–Jones pair potential is not appropriate as it does not account for the differences in pairwise interaction between different atom types. For mixed argon–xenon microclusters, the following form of the Lennard–Jones pair potential is normally used:

$$v(r) = 4\epsilon\left[(\sigma/r)^{12} - (\sigma/r)^{6}\right]$$

where r is the distance between atoms and ϵ and σ are parameters whose values depend on the types of interacting atoms. The appropriate values of ϵ and σ[14], along with the associated $r_{\min}$ and $v(r_{\min})$ for argon and xenon atoms, are tabulated in Table I, whereas the corresponding curves for $v(r)$ are shown in Figure 2.

Within this study, the following notation is used to define mixed microclusters of argon and xenon atoms:

TABLE I.
Lennard – Jones Parameters for Argon – Xenon Pair Potentials.

Interaction	σ (Å)	ε (kJ / mol)	r_{min} (Å)	v (r_{min})
Ar–Ar	3.40	1.0000	3.82	−1.00
Ar–Xe	3.65	1.4800	4.10	−1.48
Xe–Xe	4.10	1.8525	4.60	−1.85

- $Ar_i Xe_j$: a mixed microcluster containing i argon and j xenon atoms.
- $Ar_{N-n} Xe_n$: the set of microclusters $Ar_0 Xe_N, \ldots, Ar_N Xe_0$.
- $Ar_{N-n} Xe_n \mid_{i \le N \le j}$: the set of microclusters $Ar_{i-n} Xe_n, \ldots, Ar_{j-n} Xe_n$.

Intuitively, finding the minimum energy structure of a mixed microcluster would appear to be at least as difficult an optimization problem as that of finding the minimum energy structure for the corresponding pure microcluster. For example, compare the pure $Ar_5 Xe_0$ microcluster with the mixed $Ar_3 Xe_2$ microcluster. As shown by Hoare[2], the $Ar_5 Xe_0$ microcluster has a single energy minima, corresponding to a triangular bipyramid structure, slightly contracted along the symmetry axis and distended in the symmetry plane. This configuration can be constructed from the optimal $Ar_5 Xe_0$ microcluster (a tetrahedron) by adding the fifth argon atom at the apex of a tetrahedron based on a

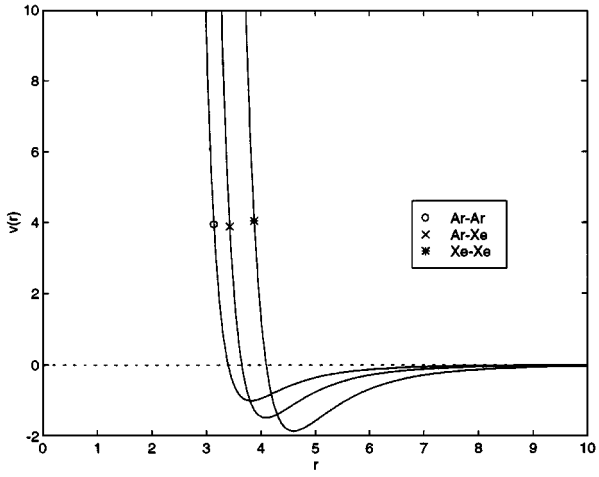

FIGURE 2. Argon–xenon Lennard–Jones pair potentials, $v(r) = 4\epsilon[(\sigma/r)^{12} - (\sigma/r)^{6}]$, where ϵ and σ are defined in Table I for each possible pair of atoms.

face of the optimal Ar_4Xe_0 microcluster and performing local optimization. Although this operation may be performed with all three faces of the Ar_5Xe_0 tetrahedron, the resulting structures are identical under symmetry operations and all result in the same energy minima for Ar_5Xe_0. Similarly, locally optimal Ar_3Xe_2 microclusters can be constructed by either adding an argon atom to the optimal Ar_2Xe_2 microcluster, or by adding a xenon atom to the optimal Ar_3Xe_1 microcluster. Using these operations, four triangular bipyramid structures may be constructed as follows:

1. An argon atom positioned at the apex of a tetrahedron based on an $\{Ar, Ar, Xe\}$ face of the optimal Ar_2Xe_2 microcluster.
2. An argon atom positioned at the apex of a tetrahedron based on an $\{Ar, Xe, Xe\}$ face of the optimal Ar_2Xe_2 microcluster.
3. A xenon atom positioned at the apex of a tetrahedron based on an $\{Ar, Ar, Xe\}$ face of the optimal Ar_3Xe_1 microcluster.
4. A xenon atom positioned at the apex of a tetrahedron based on an $\{Ar, Ar, Ar\}$ face of the optimal Ar_3Xe_1 microcluster.

Under symmetry operations, structures 1 and 3 above are identical, leaving three unique structures corresponding to three distinct local minima. Extending this argument, it would be reasonable to conjecture that the number of local minima for $Ar_{N-n}Xe_n$ is bounded below by the number of local minima for Ar_NXe_0, for all N.

OPTIMIZATION OF MIXED MICROCLUSTERS

Navon et al.[14] and Robertson et al.[15] investigated $Ar_{7-n}Xe_n$, $Ar_{13-n}Xe_n$, and $Ar_{19-n}Xe_n$ microclusters using a combination of simulated annealing and conjugate gradient descent. The approach used by Navon and Robertson was, for a microcluster containing N atoms, to start with the known structure of the Ar_NXe_0 microcluster and randomly substitute the appropriate number of Ar atoms with Xe atoms to form an initial structure, S_0, for optimization. Using a local optimizer, a minimum energy, E_0, is located near S_0. A new structure, S_1, is then generated from S_0 by randomly interchanging the position of one Ar atom with that of one Xe atom. Using a local optimizer, a minimum energy, E_1, is located near S_1. If $E_1 < E_0$, then S_1 becomes the new starting structure. If $E_1 \geq E_0$, then S_1 is accepted with Boltzmann probability as the new starting structure. This process is repeated for a fixed number of steps. The method clearly relies on the assumption that a mixed microcluster has an underlying structure which is based on that for the corresponding pure microcluster. The $Ar_{7-n}Xe_n$, $Ar_{13-n}Xe_n$, and $Ar_{19-n}Xe_n$ microclusters investigated by Navon et al.[14] were chosen because, as their pure forms, Ar_7Xe_0, $Ar_{13}Xe_0$, and $Ar_{19}Xe_0$, respectively, are particularly stable, this assumption was more likely to be valid. However, for some of the microclusters investigated in this study, the assumption was found to be invalid and the optimization method just described would be unlikely to find all minimum energy structures.

Computational Method

The computational method used in this study to optimize mixed microclusters was a parallel real-coded genetic algorithm. GAs are based on the process of natural selection where the proportion of ''fitter'' individuals in a population tends to increase at each generation. GAs operate on an encoded version of the parameters of a problem and use genetic operators such as proportional selection (based on a fitness factor), random mutation, and crossover to generate a new population from an existing population. A detailed description of GAs may be found in Goldberg.[16]

Standard (or binary coded) GAs are efficient when applied to problems whose parameters can be encoded as short, low-order schema, which are relevant to the underlying problem and relatively unrelated to schema over other fixed positions.[16] Unfortunately, optimization of microclusters is difficult for standard GAs because:

- Atomic positions are real valued parameters. Using a binary coded GA requires that these positions must be discretized so they can be coded as binary integers. To obtain an accuracy of three digits after the decimal place, for a 30-atom microcluster, requires a binary solution vector of length 1260 bits. This in turn generates a search space of approximately 10^{400} elements over which a binary coded GA can be expected to perform poorly. An additional problem is that discrete binary coded GAs sample a continuous surface at points defined by an arbitrary grid and the global minimum may, in fact, be unobtain-

able, even when a deterministic local optimizer is used to ''fine tune'' solutions (Fig. 3a shows just such a situation). It is interesting to note that, using a real-coded GA in conjunction with a local optimizer is, in effect, a variable discretization process where the discrete value is the minimum associated with the catchment basin within which the parameter lies, and the discretization interval (at that point) is the width of this catchment basin (Fig. 3b). For a real-coded GA, the global minimum is always attainable.

- In evaluating the potential energy (and hence the fitness factor) of a microcluster, the position of each atom is only meaningful in the context of the positions of all other atoms. That is, schema over different positions are not unrelated, so standard GAs can be expected to perform poorly when applied to the microcluster problem. However, as shown by Deaven and Ho,[13] if genetic operators are developed which operate in the three-dimensional space in which the microclusters exist and are able to use building blocks within the configuration, then a GA can be successfully used on the microcluster problem.

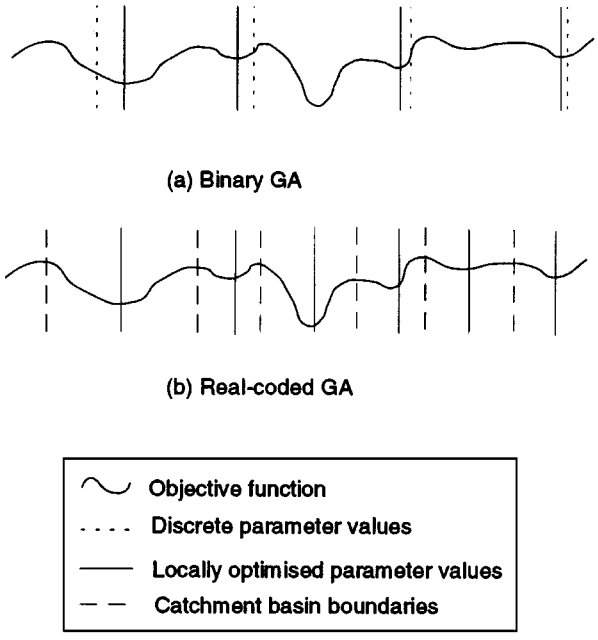

FIGURE 3. GA parameter mappings to objective function. (a) Binary parameter values and corresponding locally optimized values, and (b) real-coded parameters (mapping to the complete surface) and locally optimized values.

The parallel real-coded GA described in this article contains many of the basic features of the Deaven and Ho GA,[13,19] in particular the use of geometric crossover operators. The following definitions are used: g—generation number; p—processor number; P_g—current population for generation g; P_{pg}—the subset of P_g going to processor p; and T_g—temporary population generated from P_g. Thus, the algorithm obtained is:

	Master	**Slave(p)**
	$g = 0$	
	Initialize	**Initialize**
Next:		
	$g = g + 1$	
	Select	
	StartAll	**Wait**
	For P_{1g}	**For** P_{pg}
	Crossover	**Crossover**
	Mutate	**Mutate**
	if *finished*	
	stop all processes	
	else	
	go to *Next*	Go to *Next*

Details of the elements of this algorithm are:

- **Initialize** creates population T_g of N atom microclusters by randomly placing each atom within a cube, where the size of the cube is dependent on N. These microclusters are then locally optimized using a BFGS optimizer.
- **Select** chooses microclusters from T_g for inclusion in P_g. Selection is based on microcluster energy with the proviso that only one microcluster will be chosen with a given energy (plus or minus a small delta). At the completion of **Select**, T_g is cleared.
- **StartAll** sends a message to all slave processors to start processing, P_{pg}. The subsets, P_{pg}, are chosen such that the processing load is evenly distributed over all available processors.
- **Wait** waits for the start message from the master processor.
- **Crossover** applies crossover genetic operators to selected microclusters from P_{pg} to

generate new microclusters for inclusion in T_g. Two crossover operators for generating new microclusters were used, with equal probability. The first, χ_1, randomly rotated the coordinate system around each axis and strictly divided both parent microclusters along a plane parallel to, and a random distance above, the xy-plane, into two volume elements. The second, χ_2, randomly rotated the coordinate system around each axis and used atoms within a quadrant or an octant of the parent microclusters to construct volume elements. In both cases, new microclusters are constructed by exchanging corresponding volume elements between parents.

- **Mutate** performs BFGS local minimization, with a performance-related early termination option, on all new microclusters. In addition, with probability, p_m, one of two equally likely mutation operators was applied. Either a combination of BFGS local minimizations and APSE[17] searches was used to perform a localized random search within the structural vicinity of the new microcluster, or randomly chosen argon and xenon atoms were interchanged and a BFGS local minimization was performed. In both cases, the best microcluster found was added to T_g.

Although no formal investigations were performed to investigate the effect of changing global parameters for this algorithm, it appeared that best results were obtained with small constant-sized populations (8–12 microclusters), a low mutation probability ($\simeq 0.01$), and a high crossover probability ($\simeq 0.8$) distributed equally between χ_1 and χ_2.

Crossover operators such as χ_1 and the quadrant version of χ_2 interchange large volumes between current microclusters. Fine tuning of the microcluster was provided by the octant version of χ_2, the use of BFGS and APSE optimization, and swapping of Ar and Xe atoms within the mutation operator.

An experimental and analytical evaluation of the efficiency of these geometric operators, compared to the normal random genetic crossover operators, is presented in Pullan.[18]

Results

The GA successfully located all currently accepted global minima[14] for $Ar_{7-n}Xe_n$ and $Ar_{13-n}Xe_n$ microclusters while the results for $Ar_{19-n}Xe_n$ were generally improved. In addition, minima for the remaining microclusters in $Ar_{N-n}Xe_n \mid_{2 \le N \le 20}$ were determined by running the GA for 50 generations, at which point all minimum population energies had stabilized. The lowest energies, E, and the substitution energy, ΔE, as the Ar to Xe substitutions were performed are presented in Appendix A. The energy, E, represents an upper bound on the energy of the global minima for these systems as there is no guarantee that a GA will find the global minima. However, it should be noted that this GA, in addition to repeating the results of Navon et al.,[14] has previously located the currently accepted global minima for all $Ar_N Xe_0 \mid_{2 \le N \le 80}$ microclusters.[18]

The energy values obtained and corresponding microcluster structures are discussed in the following section.

The effectiveness of the GA in optimizing mixed microclusters is shown in Figure 4 where the minimum energy in the current population of microclusters, as a function of generation, is plotted for the optimization of the $Ar_{10}Xe_{10}$ microcluster. This pattern, with an initial sharp decrease in energy followed by a slow approach to the global minimum, was observed for all microclusters.

The number of generations required to find the currently accepted global minima for $Ar_N Xe_0 \mid_{2 \le N \le 80}$, as a function of the number of atoms in the microcluster, is shown in Figure 5. A least-

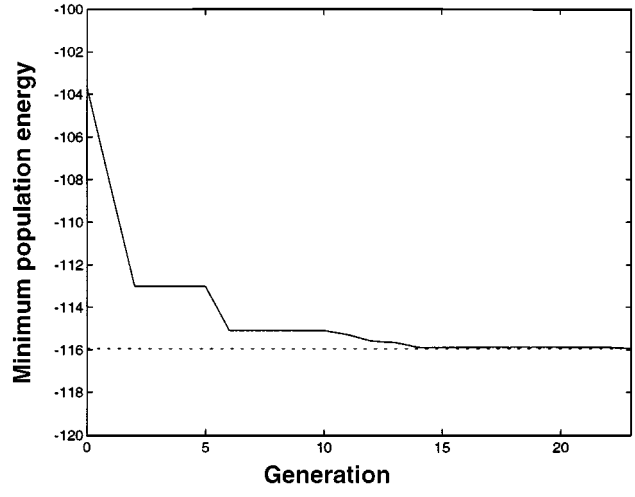

FIGURE 4. Minimum population energies while optimizing $Ar_{10}Xe_{10}$ starting from randomly generated, locally optimized, initial configurations.

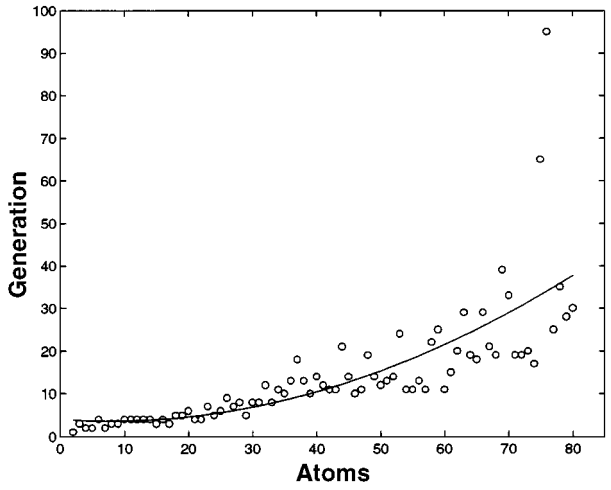

FIGURE 5. Generations required to optimize microclusters $Ar_N Xe_0 \mid_{2 \le N \le 80}$. Each point represents the number of generations required for a single optimization of each cluster.

squares fit of the data gives:

$$G = 0.0065N^2 - 0.0970N + 4.028$$

where G is the number of generations required. However, as each datapoint is the result of a single optimization run for a cluster, and as there appears to be a new trend developing for $N \geq 74$, this fit may be inappropriate for higher N.

The multiprocessor scalability of the GA is shown in Figure 6 for the $Ar_{40} Xe_0$ microcluster,

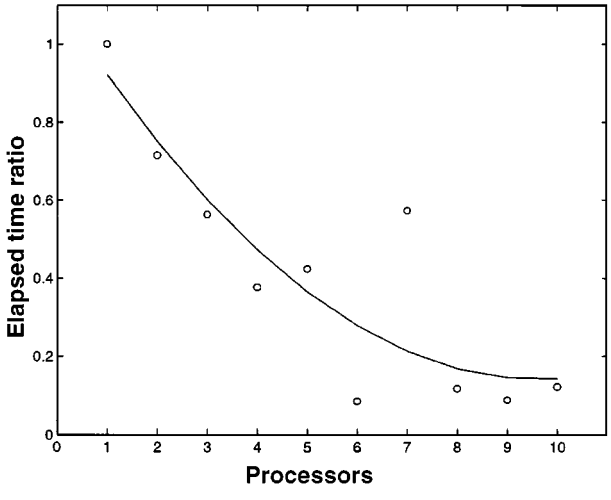

FIGURE 6. Decrease in the elapsed time to optimize $Ar_{40}Xe_0$ as the number of computer processors is increased. The elapsed time for a single processor is taken as unity and each point represents the number of generations required for a single optimization of this cluster.

optimized using from 1 to 10 processors (taking the elapsed time for the single processor case as unity). A least-squares fit of this data gives:

$$E = 0.0105P^2 - 0.2022P + 1.113$$

where P is the number of processors and E is the ratio of elapsed time for P processors to the elapsed time for a single processor.

Inefficiencies arise from normal message handling in the multiprocessor implementation and also when there is a mismatch between the population size and the number of processors. That is, the required crossover/mutation operations cannot be equally spread across available processors.

Discussion

As observed in Navon et al.,[14] in discussing the results obtained, it is important to keep in mind the relative energy minima of the three Lennard–Jones pair potentials (Table I), and the interatomic distances at which they occur. The strongest attractive interaction (lowest minima) is the *Xe–Xe* interation, whereas the weakest is *Ar–Ar*. Navon et al.[14] suggested that, as a crude model, if there are more argon than xenon atoms, then the number of *Ar–Xe* nearest neighbors should be maximized and the number of *Ar–Ar* nearest neighbors minimized. Alternatively, if there are more xenon than argon atoms then the number of *Xe–Xe* nearest neighbors should be maximized. Clearly, this model only takes into account the relative Lennard–Jones energy minima and not the interatomic distances at which they occur.

An alternative perspective, which does incorporate the different interatomic distances at which the energy minima occur, is to consider the number of atom pairs whose separation is within a small δ of the optimum ($r_{\min}$, Table I) for that atom pair. For $\delta = 0.2$ Å, N_{AA}, the count of near optimal *Ar–Ar* pairings, N_{AX}, the count of near optimal *Ar–Xe* pairings, and N_{XX}, the count of near optimal *Xe–Xe* pairings, are shown in Appendx A for all optimized $Ar_{N-n} Xe_n \mid_{2 \le N \le 20}$ microclusters. Although the value of δ is somewhat arbitrary, it is reasonable to assume that if the distance between two atoms is greater than 0.2 Å of the optimal distance for that pair, then the optimization process has not focused on optimizing the relationship between these two atoms. If we denote the minimum value of the *Ar–Ar* pair

potential by V_{AA}, that for $Ar - Xe$ by V_{AX}, and for $Xe - Xe$ by V_{XX}, then the optimization problem is approximated by:

$$\min(N_{AA}V_{AA} + N_{AX}V_{AX} + N_{XX}V_{XX})$$

Optimization studies of pure microclusters[2] have shown that the maximum possible values of N_{AA}, N_{AX}, and N_{XX}, for 2–13 atoms, are 1, 3, 6, 9, 12, 16, 19, 23, 27, 31, 36, and 42, respectively. Using these results, inspection of the actual counts presented in Appendix A shows that, when there is a relatively large number of argon atoms, N_{AX} is maximized. As a secondary effect, N_{AA} is minimized (which is equivalent to maximizing N_{XX}). Only when there are considerably more xenon than argon atoms does the focus move to maximizing N_{XX}. Intuitively, the initial maximizing of N_{AX} can be understood in terms of the relative energy minima of the different pair potentials. For example, if there are only two xenon atoms, then the maximum value of N_{XX} is one. In contrast, if the two Xe atoms are separated, then the possible values for N_{AX} have a much greater range. Even though the Xe–Xe pair has a lower potential energy minimum than the Ar–Xe, the number of possible $Ar - Xe$ pairs more than compensates. This effect is clearly seen in the optimized Ar_5Xe_2 microcluster shown in Figure 7, where the two xenon atoms were placed at the apex positions, thus maximizing N_{AX}.

Analysis of the values obtained for the substitution energy, ΔE, in Appendix A, shows that, for all $Ar_{N-n}Xe_n \mid_{2 \le N \le 9}$ microclusters, the ΔE values are generally higher for greater N and slowly decrease as Xe atoms are substituted for Ar atoms.

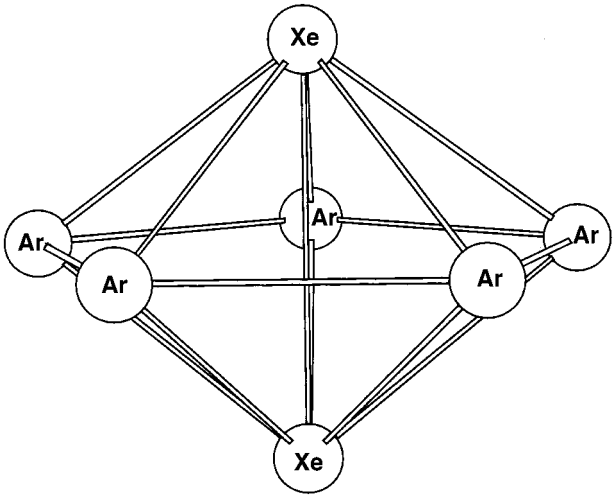

FIGURE 7. Optimized structure, Ar_5Xe_2.

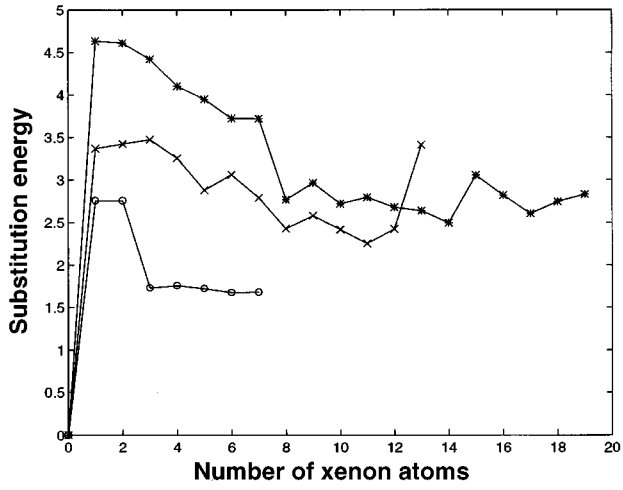

FIGURE 8. Substitution energies (ΔE) for $Ar_{7-n}Xe_n$, $Ar_{13-n}Xe_n$, and $Ar_{19-n}Xe_n$ as xenon atoms are substituted for argon atoms.

However, for all $Ar_{N-n}Xe_n \mid_{10 \le N \le 20}$ microclusters, whereas substitution of the first seven Ar atoms follows this pattern, the ΔE values are more erratic as the remaining substitutions are performed. Figure 8 shows the behavior of ΔE obtained in this study, for all $Ar_{7-n}Xe_n$, $Ar_{13-n}Xe_n$, and $Ar_{19-n}Xe_n$ microclusters. The substitution energies shown here follow the same pattern as those found in Novon et al.[14]

To determine the reasons for the observed behavior of ΔE, three microclusters were further investigated.

- Microcluster $Ar_{10-n}Xe_n$: Figure 9 shows the variation in ΔE as xenon atoms replace ar-

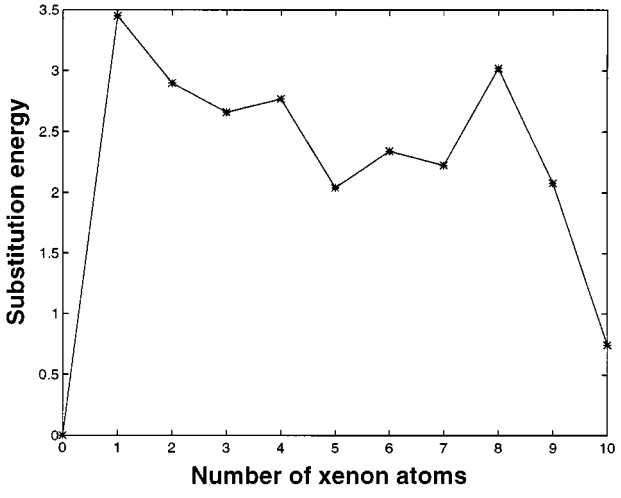

FIGURE 9. Substitution energies (ΔE) for $Ar_{10-n}Xe_n$ as xenon atoms are substituted for argon atoms.

gon atoms in the $Ar_{10-n}Xe_n$ microclusters. The first xenon atom is placed at the center of the partially constructed $Ar_{10}Xe_0$ icosahedron and, up until the sixth xenon atom, substitute argon atoms in the shell of the partial icosahedron. The structure changes when the sixth xenon is substituted in that the xenon atom at the center of the icosahedron is replaced by an argon atom (Figs. 10 and 11). This corresponds to the first increase in ΔE shown in Figure 9. As more xenon atoms are added, they are placed in the icosahedral shell which gradually envelopes the central argon atom. The second increase in ΔE occurs when the eighth xenon atom is added (Figs. 12 and 13). The rectangular base of four xenon atoms beneath the apex xenon atom in the optimized Ar_3Xe_7 microcluster has sides of length 5.83 Å and 4.71 Å. When the eighth xenon atom is added, the remaining rectangular base of four xenon atoms is able to contract to a square of side 4.91 Å which is closer to the $Xe{-}Xe$ $r_{\min}$ of 4.60. This results in a considerable increase in N_{AX}.

- Microcluster $Ar_{12-n}Xe_n$: Figure 14 shows the variation in ΔE as xenon atoms replace argon atoms in the $Ar_{12-n}Xe_n$ microclusters. The pattern followed was that the first xenon atoms substituted argon atoms in the partial icosahedral shell. The last xenon atom replaced the argon atom at the center of the icosahedron (Figs. 15 and 16). The subse-

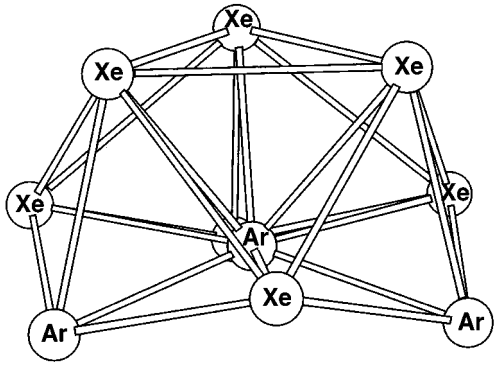

FIGURE 11. Minimum energy structure for Ar_4Xe_6.

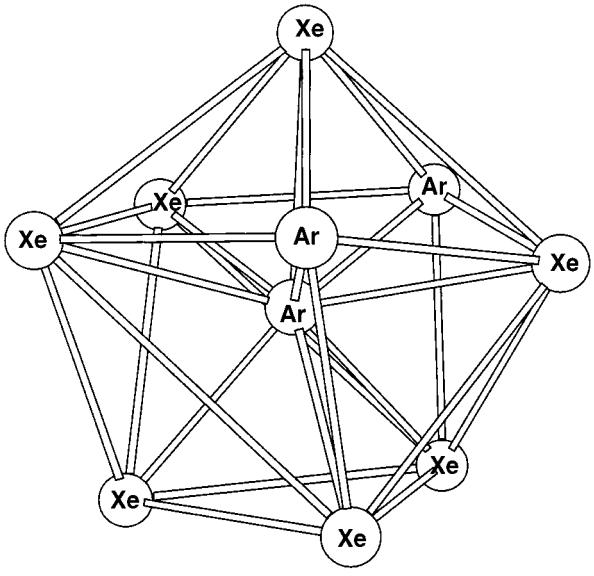

FIGURE 12. Minimum energy structure for Ar_3Xe_7.

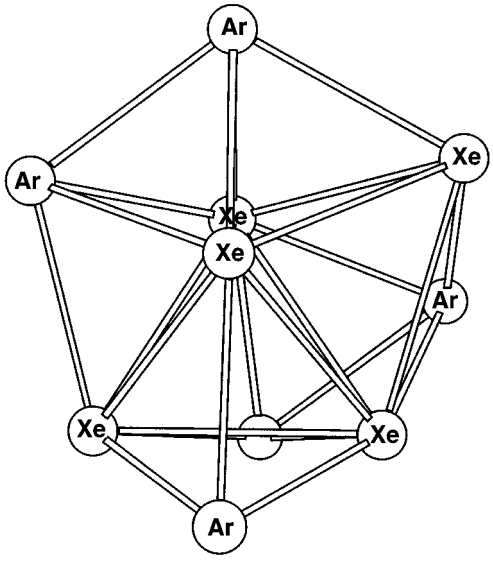

FIGURE 10. Minimum energy structure for Ar_5Xe_5.

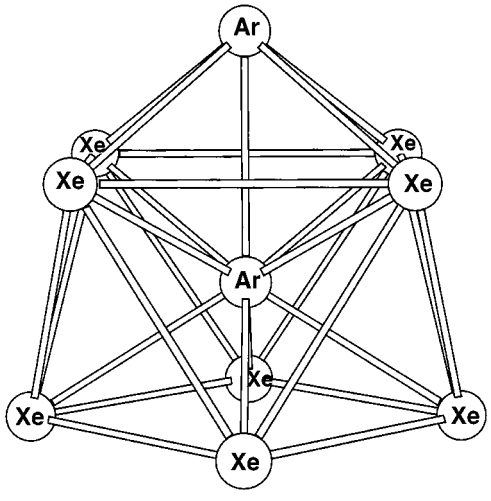

FIGURE 13. Minimum energy structure for Ar_2Xe_8.

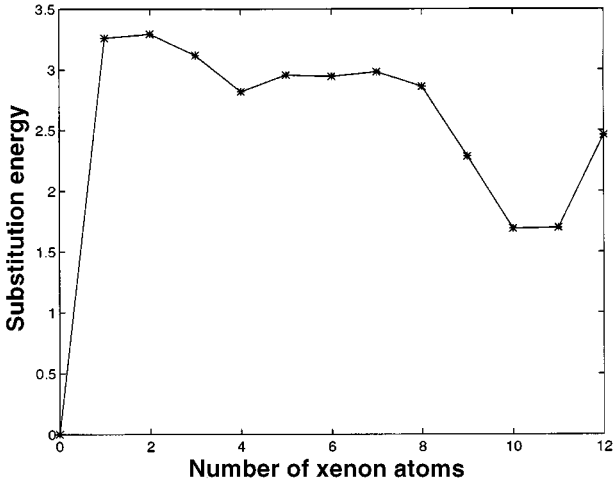

FIGURE 14. Substitution energies (ΔE) for $Ar_{12-n}Xe_n$ as xenon atoms are substituted for argon atoms.

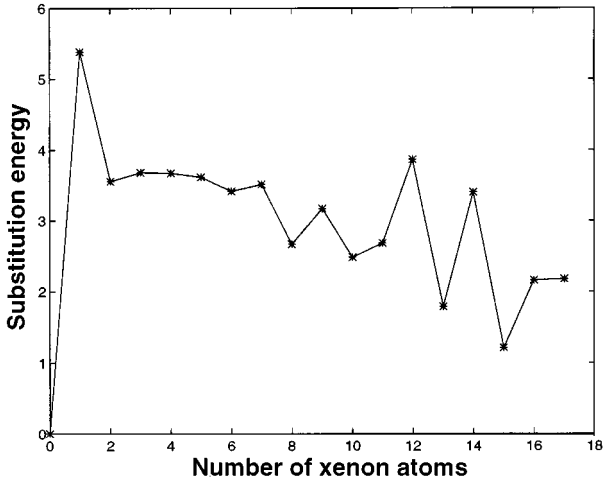

FIGURE 17. Substitution energies (ΔE) for $Ar_{17-n}Xe_n$ as xenon atoms are substituted for argon atoms.

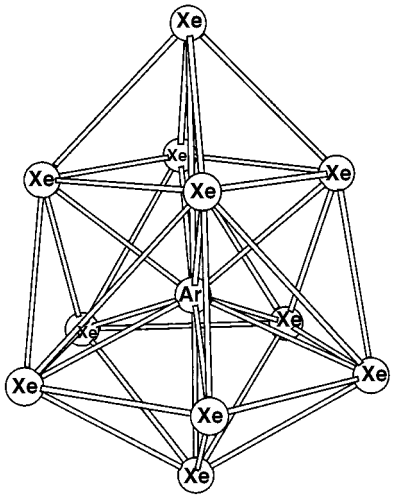

FIGURE 15. Minimum energy structure for Ar_1Xe_{11}.

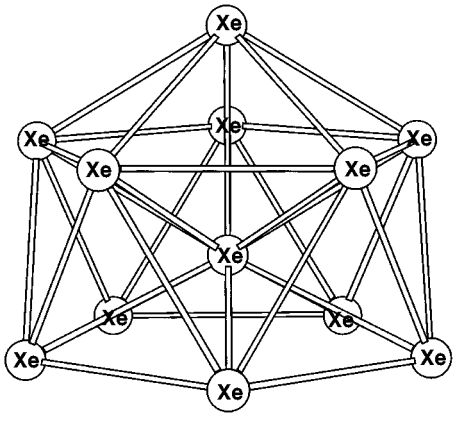

FIGURE 16. Minimum energy structure for Ar_0Xe_{12}.

quent relaxation and adjustment of the microcluster resulted in N_{XX} increasing from 25 to 36, giving the large increase in ΔE shown in Figure 14.

- Microcluster $Ar_{17-n}Xe_n$: Figure 17 shows the variation in ΔE as xenon atoms replace argon atoms in $Ar_{17-n}Xe$ microclusters. The increase in ΔE when the twelfth xenon atom is added results from a major change in structure between Ar_6Xe_{11} (Fig. 18) and Ar_5Xe_{12} (Fig. 19). At this point, the structure changes from a central xenon atom with all other argon and xenon atoms in an enclosing shell to two interpenetrating icosahedrons centered on two argon atoms. This created a significant increase in N_{AX}. The next two major increases in ΔE occur when the four-

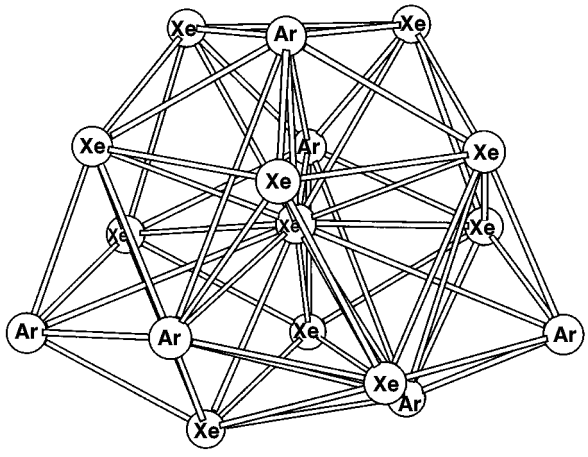

FIGURE 18. Minimum energy structure for Ar_6Xe_{11}.

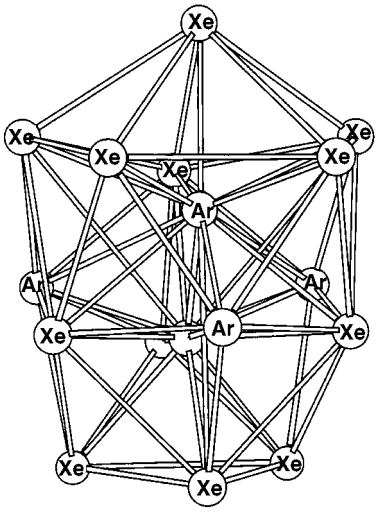

FIGURE 19. Minimum energy structure for Ar_5Xe_{12}.

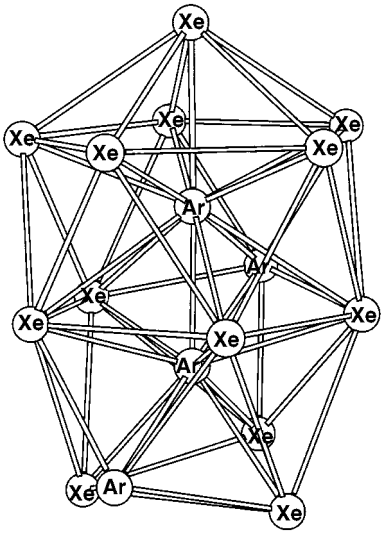

FIGURE 20. Minimum energy structure for Ar_4Xe_{13}.

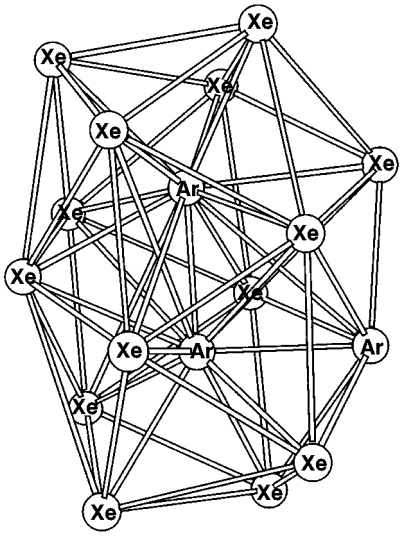

FIGURE 21. Minimum energy structure for Ar_3Xe_{14}.

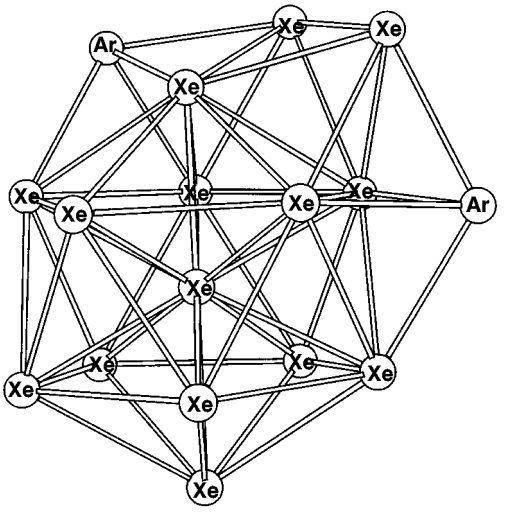

FIGURE 22. Minimum energy structure for Ar_2Xe_{15}.

teenth and sixteenth xenon atoms are added. As in the $Ar_3\,Xe_7$ to $Ar_2\,Xe_8$, these allowed a rectangular base of xenon atoms to transform to a square whose sides were closer to $r_{\min}$ for $Xe - Xe$, thus increasing N_{XX}.

Conclusions

In this article, an investigation designed to determine the energy-optimized structures of Lennard–Jones microclusters containing a mix of argon and xenon atoms has been presented. A GA, whose genetic operators operated in the problem space, was able to find these structures efficiently. In common with all GAs, it explored the search domain in parallel using all microclusters in the current population as starting points. The crossover and mutation genetic operators functioned at a number of levels when generating new microclusters. At a high level, crossover operators such as χ_1 and the hemisphere version of χ_2 interchanged large volumes between current microclusters. Fine tuning of the microcluster was provided by the quadrant and octant version of χ_2, the use of BFGS and APSE optimization, and the swapping of Ar and Xe atoms within the mutation operator.

An important feature of the GA is that, as it always starts from randomly generated structures and has no bias toward any particular structure, it will perform a more complete search of the domain of possible structures. Alternative methods, which start from a particular structure, are likely to have an inherent bias toward that structure and are less able to find different structures that may have lower energy.

The energies, substitution energies, and atom pair counts have been tabulated for all $Ar_{N-n}Xe_n \mid_{2 \le N \le 20}$ microclusters. In addition, further investigation of the optimized structures for $Ar_{10-n}Xe_n$, $Ar_{12-n}Xe_n$ and $Ar_{17-n}Xe_n$ microclusters was performed to determine the reasons for the observed changes in substitution energy.

Acknowledgments

The author thanks Graham Wood and the anonymous referees for their many critical and constructive comments while preparing this paper.

Appendix A: Microcluster Properties

The following table contains:

- The optimized energies for all $Ar_{N-n}Xe_n \mid_{2 \le N \le 20}$ microclusters.
- The substitution energy, ΔE, as Xe atoms are substituted for Ar atoms in each microcluster. ΔE is tabulated as an absolute value.
- The counts of Ar–Ar, Ar–Xe, and Xe–Xe atom pairings where the distance between the atoms is within 0.2 Å of $r_{\min}$ for the respective atom types.

n	E	ΔE	N_{AA}	N_{AX}	N_{XX}
	$Ar_{2-n}Xe_n$				
0	−1.0000		1	0	0
1	−1.4800	0.4800	0	1	0
2	−1.8525	0.3725	0	0	1
	$Ar_{3-n}Xe_n$				
0	−3.0000		3	0	0
1	−3.9600	0.9600	1	2	0
2	−4.8125	0.8525	0	2	1
3	−5.5575	0.7450	0	0	3
	$Ar_{4-n}Xe_n$				
0	−6.0000		6	0	0
1	−7.4400	1.4400	3	3	0
2	−8.7725	1.3325	1	4	1
3	−9.9975	1.2250	0	3	3
4	−11.1150	1.1175	0	0	6
	$Ar_{5-n}Xe_n$				
0	−9.1039		9	0	0
1	−11.0176	1.9137	5	4	0
2	−12.8290	1.8114	2	6	1
3	−14.5408	1.7118	0	6	3
4	−15.6858	1.1450	0	3	6
5	−16.8649	1.1791	0	0	9
	$Ar_{6-n}Xe_n$				
0	−12.7121		12	0	0
1	−14.7512	2.0391	8	4	0
2	−16.9602	2.2090	3	8	1
3	−18.7090	1.7488	1	8	3
4	−20.5018	1.7928	0	8	4
5	−21.9889	1.4871	0	4	8
6	−23.5491	1.5602	0	0	12
	$Ar_{7-n}Xe_n$				
0	−16.5054		15	0	0
1	−19.2622	2.7568	10	6	0
2	−22.0179	2.7557	5	9	1
3	−23.7468	1.7289	3	10	2
4	−25.5027	1.7559	1	10	4
5	−27.2248	1.7221	0	8	7
6	−28.8997	1.6749	0	4	12
7	−30.5762	1.6765	0	0	15
	$Ar_{8-n}Xe_n$				
0	−19.8215		19	0	0
1	−23.0058	3.1843	12	7	0
2	−25.8141	2.8083	7	11	1
3	−28.0031	2.1890	4	12	2
4	−30.1491	2.1460	2	11	5
5	−31.9569	1.8078	0	11	7
6	−33.6846	1.7277	0	7	12
7	−35.3818	1.6972	0	3	16
8	−36.7193	1.3375	0	0	19
	$Ar_{9-n}Xe_n$				
0	−24.1134		23	0	0
1	−27.5466	3.4332	15	8	0
2	−30.3876	2.8410	10	12	1
3	−32.9050	2.5174	6	14	3
4	−35.1329	2.2279	4	13	6
5	−37.3987	2.2658	2	12	9
6	−39.1971	1.7984	1	10	12
7	−41.0267	1.8296	0	8	15
8	−42.8423	1.8156	0	4	19
9	−44.6700	1.8277	0	0	23

n	E	ΔE	N_{AA}	N_{AX}	N_{XX}
$Ar_{10-n}Xe_n$					
0	−28.4225		27	0	0
1	−31.8734	3.4509	12	9	0
2	−34.7706	2.8972	7	13	1
3	−37.4314	2.6608	5	15	3
4	−40.2013	2.7699	4	16	6
5	−42.2426	2.0413	2	15	9
6	−44.5857	2.3431	3	15	9
7	−46.8097	2.2240	2	8	11
8	−49.8288	3.0191	1	12	12
9	−51.9091	2.0803	0	9	18
10	−52.6528	0.7437	0	0	27
$Ar_{11-n}Xe_n$					
0	−32.7660		31	0	0
1	−36.1896	3.4236	19	10	0
2	−39.1815	2.9919	14	14	1
3	−42.1373	2.9558	10	17	3
4	−45.1324	2.9951	4	18	6
5	−47.6269	2.4945	0	18	9
6	−50.5539	2.9270	6	18	8
7	−53.3974	2.8435	4	16	10
8	−56.9554	3.5580	0	16	8
9	−58.6126	1.6572	0	12	16
10	−60.2662	1.6536	0	9	20
11	−60.6990	0.4328	0	0	31
$Ar_{12-n}Xe_n$					
0	−37.9676		36	0	0
1	−41.2283	3.2607	30	6	0
2	−44.5236	3.2953	24	12	0
3	−47.6411	3.1175	19	16	1
4	−50.4576	2.8165	15	19	2
5	−53.4130	2.9554	11	22	3
6	−56.3567	2.9437	8	18	7
7	−59.3386	2.9819	5	20	10
8	−62.1998	2.8612	3	18	12
9	−64.4855	2.2857	1	16	17
10	−66.1764	1.6909	0	13	21
11	−67.8740	1.6976	0	9	25
12	−70.3350	2.4610	0	0	36
$Ar_{13-n}Xe_n$					
0	−44.3268		39	0	0
1	−47.6968	3.3700	36	6	0
2	−51.1213	3.4245	19	16	1
3	−54.5957	3.4744	24	18	0
4	−57.8543	3.2586	19	22	1
5	−60.7363	2.8820	17	20	5
6	−63.7979	3.0616	12	24	6
7	−66.5918	2.7939	10	22	10
8	−69.0209	2.4291	3	23	13
9	−71.6010	2.5801	5	20	17
10	−74.0185	2.4175	2	20	20
11	−76.2746	2.2561	1	11	25
12	−78.7008	2.4262	0	1	36
13	−82.1154	3.4146	0	0	39
$Ar_{14-n}Xe_n$					
0	−47.8452		45	0	0
1	−51.6528	3.8076	38	7	0
2	−55.2653	3.6125	32	12	1
3	−58.8911	3.6258	27	15	3
4	−62.3267	3.4356	21	21	3
5	−65.5107	3.1840	16	25	4
6	−68.6972	3.1865	12	27	6
7	−71.5258	2.8286	10	25	10
8	−73.9865	2.4607	7	25	13
9	−76.5749	2.5884	5	23	17
10	−79.0019	2.4270	3	19	21
11	−81.2590	2.2571	1	14	25
12	−83.7123	2.4533	0	7	36
13	−87.1603	3.4480	0	3	42
14	−88.6800	1.5197	0	0	45
$Ar_{15-n}Xe_n$					
0	−52.3227		49	0	0
1	−56.3670	4.0443	30	14	0
2	−60.1992	3.8322	33	14	1
3	−63.9532	3.7540	28	17	3
4	−67.6800	3.7268	24	20	4
5	−71.1313	3.4513	17	26	4
6	−74.3084	3.1771	11	30	5
7	−77.1841	2.8757	11	28	10
8	−79.6808	2.4967	0	32	12
9	−82.2536	2.5728	5	26	17
10	−84.7267	2.4731	4	23	21
11	−86.9356	2.2089	1	17	25
12	−89.5321	2.5965	1	10	35
13	−92.9570	3.4249	1	6	41
14	−94.9799	2.0229	0	4	44
15	−97.0191	2.0392	0	0	48
$Ar_{16-n}Xe_n$					
0	−56.8158		53	0	0
1	−61.8505	5.0347	33	14	0
2	−65.1729	3.3224	29	18	0
3	−68.8390	3.6661	27	19	3
4	−72.5794	3.7404	25	22	3
5	−76.1583	3.5789	19	28	3
6	−79.6076	3.4493	13	31	7
7	−82.6623	3.0547	10	31	10
8	−85.1669	2.3458	8	29	14
9	−87.7763	2.7682	4	30	16
10	−90.2711	2.4948	2	26	19

n	E	ΔE	N_{AA}	N_{AX}	N_{XX}
11	−92.8687	2.5976	1	23	24
12	−95.5958	2.7271	1	24	16
13	−98.5781	2.9823	0	9	40
14	−101.0880	2.5101	0	8	43
15	−103.2260	2.1382	0	4	47
16	−105.3870	2.1609	0	0	51
$Ar_{17-n}Xe_n$					
0	−61.3180		57	0	0
1	−66.7034	5.3854	36	14	0
2	−70.2609	3.5575	31	19	1
3	−73.9456	3.6847	26	22	3
4	−77.6197	3.6741	28	25	3
5	−81.2377	3.6180	22	31	3
6	−84.6540	3.4163	17	30	7
7	−88.1712	3.5172	10	34	10
8	−90.8381	2.6669	8	33	11
9	−94.0120	3.1739	5	32	16
10	−96.4962	2.4842	3	29	20
11	−99.1802	2.6840	2	26	23
12	−103.0480	3.8679	3	30	22
13	−104.8350	1.7873	2	22	27
14	−108.2390	3.4039	1	21	32
15	−109.4510	1.2115	0	8	45
16	−111.6100	2.1595	0	4	49
17	−113.7890	2.1788	0	0	54
$Ar_{18-n}Xe_n$					
0	−66.5310		61	0	0
1	−71.6344	5.1034	42	14	0
2	−75.4300	3.7956	43	16	0
3	−79.6966	4.2666	38	22	1
4	−83.7028	4.0062	32	26	3
5	−87.5703	3.8675	26	30	5
6	−91.2575	3.6872	20	36	5
7	−94.1626	2.0879	17	37	7
8	−97.2132	3.8678	14	38	9
9	−99.9746	2.7614	11	38	12
10	−102.9080	2.9334	9	34	16
11	−105.6790	2.7706	7	31	20
12	−108.2810	2.6019	0	26	31
13	−111.0780	2.7979	2	29	27
14	−113.5770	2.4987	1	25	32
15	−116.1860	2.6091	2	12	43
16	−118.2490	2.0625	1	12	47
17	−120.4410	2.1925	0	3	53
18	−123.4810	3.0398	0	0	56
0	−72.6620		67	0	0
1	−77.2985	4.6365	59	8	0
2	−81.9088	5.6103	51	16	0
3	−86.3286	4.4198	44	22	1
4	−90.4325	4.1039	38	26	3
5	−94.3813	3.9488	32	30	5
6	−98.1058	3.7245	26	36	5
7	−101.8270	3.7215	20	42	5
8	−104.5980	2.7704	17	42	8
9	−107.5650	2.9672	15	38	12
10	−110.2860	2.7211	13	35	16
11	−113.0830	2.7974	11	38	17
12	−115.7640	2.6805	9	35	22
13	−118.4020	2.6382	7	34	26
14	−120.8970	2.4949	6	27	32
15	−123.9530	3.0556	5	17	43
16	−126.7740	2.8215	3	15	47
17	−129.3820	2.6074	1	12	49
18	−132.1260	2.7448	0	7	51
19	−134.9560	2.8297	0	0	65
$Ar_{19-n}Xe_n$					
0	−77.1794		70	0	0
1	−81.8554	4.6760	63	8	0
2	−86.5218	4.6664	53	16	1
3	−91.1201	4.5983	45	24	1
4	−95.1858	4.0657	39	28	3
5	−99.2034	4.0176	35	34	2
6	−102.8620	3.6584	27	38	5
7	−106.6060	3.7443	21	44	5
8	−109.8870	3.2808	17	45	8
9	−113.0180	3.1308	14	44	9
10	−115.9530	2.9353	12	41	14
11	−118.8340	2.8805	11	38	19
12	−121.5280	2.6944	9	36	22
13	−124.2350	2.7075	7	34	25
14	−126.7900	2.5545	5	30	30
15	−129.8970	3.1072	5	18	42
16	−132.8010	2.9044	3	17	45
17	−135.4560	2.6540	1	15	48
18	−138.1490	2.6934	0	9	52
19	−141.0400	2.8911	0	2	62
20	−143.3990	2.3591	0	0	62

References

1. B. A. Hendrikson, *Cornell Theory Center Technical Report CTC90TR28*, 1990.
2. M. R. Hoare, *Adv. Chem. Phys.*, **40,** 49 (1979).
3. A. Liao, *Cornell Theory Center Technical Report CTC94TR190*, 1994.
4. J. A. Northby, *J. Chem. Phys.*, **87,** 6166 (1987).

5. M. R. Hoare and P. Pal, *Adv. Phys.*, **20,** 161 (1971).
6. M. R. Hoare and J. A. McInnes, *Adv. Phys.*, **32,** 791 (1983).
7. M. R. Hoare and J. McInnes, *Faraday Disc. Chem. Soc.*, **61,** 12 (1976).
8. L. T. Wille, *Chem. Phys. Lett.*, **133,** 5 (1987).
9. G. Xue, *J. Global Opt.*, **4,** 187 (1994).
10. B. Hartke, *J. Phys. Chem.*, 97, 9973 (1993).
11. J. Mestres and G. E. Scuseria, *J. Comput. Chem.*, **16,** 729 (1995).
12. S. K. Gregurick, M. H. Alexander, and B. Hardtke, *J. Chem. Phys.*, **104,** 2684 (1996).
13. D. M. Deaven and K. M. Ho, *Phys. Rev. Lett.*, **75,** 288 (1995).
14. I. M. Navon, F. B. Brown, and D. H. Robertson, *Comp. Chem.*, **14,** 305 (1990).
15. D. H. Robertson, F. B. Brown, I. M. Navon, and I. M. Brown, *J. Chem. Phys.*, **90,** 3221 (1989).
16. D. Goldberg, *Genetic Algorithms in Search, Optimization and Machine Learning*, Addison-Wesley, Reading, MA, 1989.
17. W. J. Pullan, *Austral. Comput. J.* (in press).
18. W. J. Pullan, *Technical Report MC96-002*, Department of Mathematics and Computing, Central Queensland University, 1996.
19. D. M. Deaven, N. Tit, J. R. Morris, K. Ho, Structural Optimization of Lennard–Jones Clusters by a Genetic Algorithm, preprint, 1996.